2

The atmospheres of extrasolar planets

2.1 Introduction

In this chapter we examine what can be learned about extrasolar planet atmospheres by concentrating on a class of planets that *transit* their parent stars. As discussed in the previous chapter, one way of detecting an extrasolar planet is by observing the drop in stellar intensity as the planet passes in front of the star. A transit represents a special case in which the geometry of the planetary system is such that the planet's orbit is nearly edge-on as seen from Earth. As we will explore, the transiting planets provide opportunities for detailed follow-up observations that allow physical characterization of extrasolar planets, probing their bulk compositions and atmospheres.

2.2 The Primary Eclipse

The vast majority of the currently-known extrasolar planets have been detected using the radial velocity technique.† As detailed in the previous chapter, the radial velocity method searches for periodic motion of a star caused by the gravitational pull of an orbiting companion. Figure 1.1 shows a sketch of a typical periodic radial velocity signal and the basic geometry of the planetary system. This method is sensitive only to movement of the star towards and away from the observer, that is, along the line of sight from the system to the observer on Earth. Thus, radial velocity observations provide only a determination of the *minimum* mass M of the planet, and the orbital inclination i of the system remains unknown, as in

$$M = M_p \sin i, \tag{2.1}$$

where M_p is the *true* mass of the planet. (See Section 1.2 for further details.)

† An up-to-date reference and catalog of all known extrasolar planets can be found at `http://vo.obspm.fr/exoplanetes/encyclo/encycl.html`

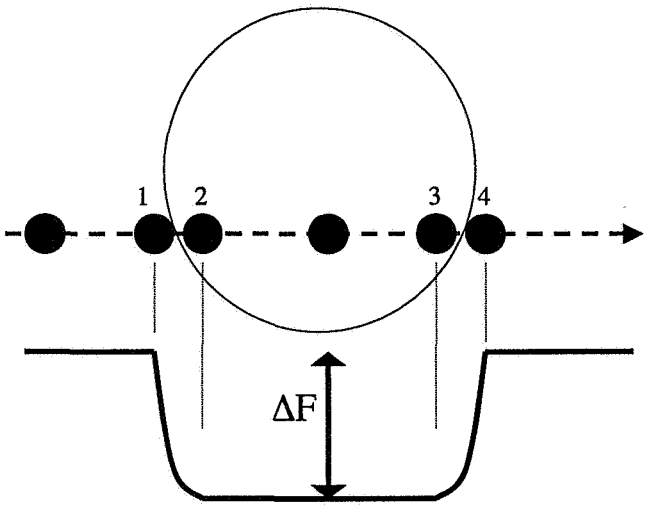

Fig. 2.1. Sketch showing a planet crossing the disk of its parent star. Transit light curve shown below.

The *primary eclipse*, or transit, occurs when the planet's orbit happens to be nearly edge-on as seen from Earth. This means that the planet periodically crosses in front of the star as it orbits, and we detect this as a decrease in the light from the star that occurs once per planet revolution, as indicated schematically in Figure 2.1. The dimming is typically a few percent or less for the currently known transiting planets. In this geometry, the orbital inclination is now known to be $\sim 90°$ (and can be determined precisely from the details of the transit light curve). We can therefore derive the true planetary mass, M_p, from Equation 2.1.

A number of other physical parameters of the planet and star can be derived from the shape of the light curve (Seager and Mallén-Ornelas, 2003). The depth of the transit ΔF (i.e., the change in flux from outside transit to during transit, as shown in Figure 2.1) is directly proportional to the ratio of the area of the planetary disk to the area of the stellar disk. That is,

$$\Delta F \equiv \frac{F_{\text{out of transit}} - F_{\text{transit}}}{F_{\text{out of transit}}} = \frac{A_p}{A_*} = \left(\frac{R_p}{R_*}\right)^2, \tag{2.2}$$

where F represents the total flux, A is the area of the disk (planet or star), and R is the radius (planet or star). With a stellar mass-radius relation, it is possible to derive both the planetary and stellar radii simultaneously. With the planetary mass M_p and radius R_p, one can immediately calculate

the average density of the planet from

$$\rho = \frac{M_p}{\frac{4}{3}\pi R_p^3}. \tag{2.3}$$

The discovery of transiting planets allowed a direct measurement of the true mass, radius, and density of planets outside the solar system for the first time. The planetary radius is key to determining the reflection and thermal emission of the planets from flux measurements. The density measurements derived from transit observations indicate that all but one of the transiting planets are hydrogen-helium gas giants, similar in bulk composition to Jupiter and Saturn in our own Solar System.

When the planet is in front of the star, the planet's atmosphere appears as an annulus surrounding the planetary disk, and some of the starlight passes through this annulus to the observer. The detection of starlight that has passed through the transiting planet's atmosphere in this manner is called *transmission spectroscopy*. By measuring how much starlight is transmitted as a function of wavelength, we can learn about the atomic and molecular species present in the planet's atmosphere, providing a much greater wealth of information than simply the average density and bulk composition. We introduce the broad study of spectroscopy in Section 2.5 and discuss recent observations of transiting planets using transmission spectroscopy in Section 2.7.

2.3 The Secondary Eclipse

A planet that crosses in front of its parent star will disappear behind the star later in its orbit. This disappearance is called the *secondary eclipse*. For a circular orbit, the secondary eclipse occurs exactly one-half of an orbital period after the primary eclipse. However, for a non-circular orbit, the secondary eclipse can occur earlier or later (depending on the eccentricity and the orientation of the orbit), and its duration can differ from that of the primary eclipse (Charbonneau, 2003). In addition to clues about the eccentricity of the planet's orbit from the secondary eclipse timing and duration, the secondary eclipse yields information about the nature of the planet's atmosphere.

For example, in visible light, the secondary eclipse probes the amount of starlight reflected by the planet's atmosphere (called the *albedo*). In the infrared, however, it measures the direct thermal emission (or intrinsic heat output) of the planet. In neither case does this imply imaging the planet;

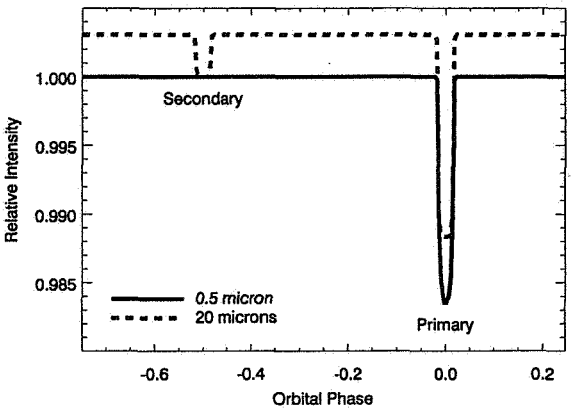

Fig. 2.2. Comparison of primary and secondary eclipses in the visible and infrared for the thermal emission of the planet HD 209458 b. These curves were calculated from a simple model that assumes the star and planet emit blackbody radiation only.

rather, the idea is to observe the total energy output of the system (star + planet) and attempt to detect a decrease as the planet is hidden from view.

Figure 2.2 illustrates this decrease in the total energy output of the system during secondary eclipse and shows that the thermal emission of the planet may be detectable at infrared wavelengths using this technique. The basic situation is that the incident starlight (which peaks in the visible for a Sun-like star) is absorbed and reprocessed by the planet's atmosphere, and some of that radiation is later emitted at infrared wavelengths. The figure shows the thermal emission of the planet HD 209458 b relative to its parent star. This calculation assumes that both the star and planet emit only blackbody radiation (Equation 2.6), and it assumes that the planet emits uniformly in both hemispheres. In the visible region (solid curve), the secondary eclipse is undetectable, both because the planet has virtually no emission at these wavelengths and because the reflected light from the planet is $\ll 0.01\%$ of the stellar output. However, as the figure shows, the situation is quite different at 20 μm. The total intensity *relative to the star* is higher outside of the eclipse, because the planet has a small but measurable intrinsic energy output at this wavelength. The secondary eclipse appears as a dip of $\sim 0.3\%$ in the total intensity as the planet is hidden by the star.

The eclipse depths at visible and infrared wavelengths can be estimated

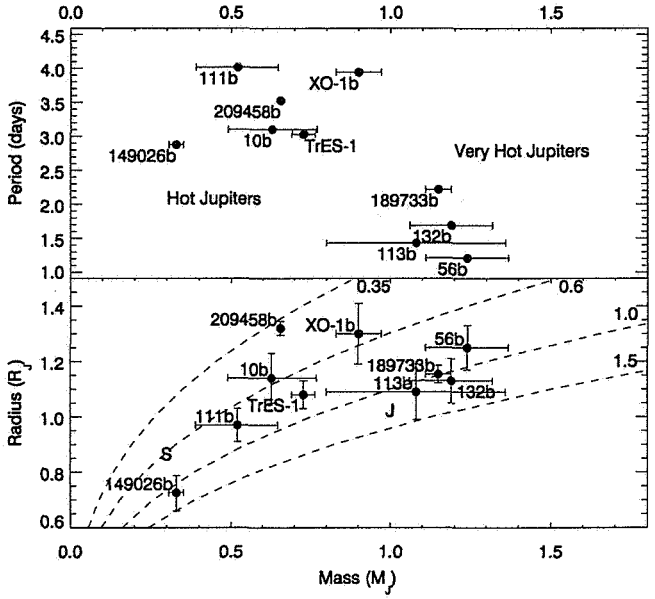

Fig. 2.3. The ten currently-known transiting planets, as a function of planetary mass. The upper panel shows the period vs. mass, and the lower panel shows radius vs. mass. Dashed curves indicate curves of constant density in g/cm^3. For comparison, Jupiter and Saturn are shown, marked by 'J' and 'S', respectively.

with the following flux ratios. For reflected light,

$$\frac{F_p}{F_*} = A_g \left(\frac{R_p}{a}\right)^2, \tag{2.4}$$

where A_g is the geometric albedo (the fraction of incident radiation scattered back into space when the planet is in full phase), R_p is the planetary radius, and a is the orbital semi-major axis. For thermal emission,

$$\frac{F_p}{F_*} = \frac{T_p}{T_*} \left(\frac{R_p}{R_*}\right)^2, \tag{2.5}$$

where T_p and T_* are the planet and star effective temperatures (see equation 2.19 for an estimate of T_p). Here we have used the approximation for the Wien tail of the blackbody flux whereby the flux ratio translates into a temperature ratio.

Table 2.1. *Physical properties of transiting extrasolar planets.*

Planet	Period (days)	Radius (R_J)	Mass (M_J)	T_* (K)	T_{eq} [1] (K)
OGLE-TR-56b[2,3]	1.212	1.25 ± 0.08	1.24 ± 0.13	6119	1929
OGLE-TR-113b[2,4]	1.432	1.09 ± 0.10	1.08 ± 0.28	4804	1234
OGLE-TR-132b[5,6]	1.690	1.13 ± 0.08	1.19 ± 0.13	6411	1933
HD 189733 b[7,8]	2.219	1.154 ± 0.032	1.15 ± 0.04	5050	1096
HD 149026 b[9,10]	2.876	$0.726\ ^{+0.062}_{-0.066}$	0.33 ± 0.023	6147	1593
TrES-1[2,11,12]	3.030	1.08 ± 0.05	0.729 ± 0.036	5226	1059
OGLE-TR-10b[2,13,14]	3.101	1.14 ± 0.09	0.63 ± 0.14	6075	1402
HD 209458 b[2,15,16]	3.525	1.320 ± 0.025	0.657 ± 0.006	6117	1363
XO-1b[17]	3.942	1.30 ± 0.11	0.90 ± 0.07	5750	1148
OGLE-TR-111b[2,18]	4.016	0.97 ± 0.06	0.52 ± 0.13	5044	935

[1]Calculated from Equation 2.19 with $f = 1$ and $A_B = 0.3$; [2] (Santos *et al.*, 2006); [3] (Torres *et al.*, 2004); [4] (Konacki *et al.*, 2004); [5] (Bouchy *et al.*, 2004); [6] (Moutou *et al.*, 2004); [7] (Bouchy *et al.*, 2005); [8] (Bakos *et al.*, 2006); [9] (Sato *et al.*, 2005); [10] (Charbonneau *et al.*, 2005); [11] (Laughlin *et al.*, 2005); [12] (Alonso *et al.*, 2004); [13] (Konacki *et al.*, 2005); [14] (Holman *et al.*, 2005); [15] (Knutson *et al.*, 2006); [16] (Winn *et al.*, 2005); [17] (McCullough *et al.*, 2006); [18] (Pont *et al.*, 2004);

2.4 Characteristics of Known Transiting Planets

A total of *ten* transiting extrasolar planets have been discovered as of May 2006. Their physical characteristics are given in Table 2.1, and they are plotted in Figure 2.3. The upper panel (period vs. mass) illustrates the two groups of transiting planets. The 'hot Jupiters' (to the upper left of the plot) have masses smaller than that of Jupiter and orbital periods greater than ~2.5 days. This name is something of a misnomer, since the so-called hot Jupiters are quite different from our own Jupiter—because of the fact that they orbit at such small orbital distances, they are much hotter and therefore have different chemical species present in their atmospheres. The other group, often called the 'very hot Jupiters,' is characterized by planets that orbit much closer to their parent stars (with orbital periods less than 2.5 days) and are more massive than Jupiter. These two dynamically distinct groups of planets may have different evolutionary histories, possibly resulting from different migration mechanisms (Gaudi *et al.*, 2005), and thus could potentially have very different atmospheric properties. We now have one bright planet from each group—HD 209458 b and HD 198733 b—

allowing us to compare observations of the two planets and gain insights into their atmospheric structure and evolutionary history.

The lower panel of Figure 2.3 shows the radius of each planet vs. mass. The dashed curves indicating constant density provide context for understanding the bulk composition of the planets. For example, most of the transiting planets are similar in average density to Jupiter ($\rho = 1.33$ g/cm^2) and Saturn ($\rho = 0.69$ g/cm^2). However, these 'close-in' extrasolar planets are likely to be quite different from our own Jupiter, due to the fact that they are much closer in to their stars. At orbital distances of $a < 0.1$ AU (by comparison, Mercury is at $a \sim 0.38$ AU), these planets are bombarded by radiation from their parent stars and are therefore expected to be hot ($T > 1000$ K). Jupiter, at 5 AU from the Sun, has a blackbody temperature of only 110 K. Because of the large temperature difference, we expect the atmospheric composition of the hot Jupiters to be significantly different from that of Jupiter. For example, at low temperatures ($T < 1000$ K), chemical equilibrium calculations show that carbon is mostly present in the form of CH_4, while at higher temperatures it appears as CO (Burrows and Sharp, 1999).

Finally, from Figure 2.3, we note that not all of the known transiting planets have densities similar to Jupiter and Saturn. The most extreme example is HD 209458 b, with an average density of $\sim$0.35 g/cm^2. This planet was the first one found to exhibit a transit (Charbonneau *et al.*, 2000; Henry *et al.*, 2000), although it was originally detected using the radial velocity method (Mazeh *et al.*, 2000). Since then, it has been observed extensively from the ground and from space, as we shall discuss further in Section 2.7. From the beginning, it was unclear why the planet appears to have a larger radius than is predicted by theory (Burrows *et al.*, 2000; Burrows *et al.*, 2003), and this remains one of the unanswered questions in the field today (Winn and Holman, 2005).

2.5 Spectroscopy

We now turn from a general discussion of the transiting planets to the specific topic of spectroscopy and the radiative transfer equation. By studying the spectroscopy of extrasolar planets, we can gain key insights into the atmospheric composition, temperature, and structure of these planets. We begin this section by introducing the Planck blackbody law, which describes the thermal emission of an object in the absence of scattering or absorbing particles, and move to the radiative transfer equation, which does account for the effects of scattering and absorption. The radiative transfer equation

governs the interaction of energy (in the form of emitted or absorbed radiation) with matter (in this case the particles that make up the planetary atmosphere). In Section 2.6 we give an overview of how models of planetary atmospheres are computed. Spectra derived from such models help interpret observational results and facilitate the design of future planet atmosphere detection instruments.

At the most basic level we can approximate the star and planet as blackbodies. In that case, where we ignore the details of the atmosphere, the emission is given by Planck's blackbody law:

$$B_\lambda(T) = \frac{2hc^2}{\lambda^5(e^{hc/\lambda kT} - 1)}, \tag{2.6}$$

where λ is wavelength, c is the speed of light in vacuum, k is Boltzmann's constant, T is the temperature of the blackbody, and h is Planck's constant. For a stellar or planetary atmosphere which contains a variety of different species that absorb, emit, and scatter radiation, however, the blackbody law is not sufficient to describe the resulting spectrum, and it becomes necessary to understand how matter interacts with the radiation.

Following convention, we begin by considering a pencil of radiation traveling through a medium. The energy in the beam is given by

$$dE_\nu = I_\nu \cos\theta \, dA \, d\Omega \, d\nu \, dt, \tag{2.7}$$

where ν is wavenumber $(1/\lambda)$, I_ν is the monochromatic (spectral) *radiance* (sometimes called intensity), θ is the angle from the normal to the surface, dA is a differential area element intercepting the beam, Ω is the solid angle in steradians, and t is time.

Next, we explicitly describe how the radiation beam changes as it interacts with matter (of density ρ), traveling through a distance ds:

$$dI_\nu = -k_\nu \, \rho \, I_\nu \, ds + j_\nu \, \rho \, ds. \tag{2.8}$$

The first term on the right hand side represents the amount of radiation removed from the beam (extinction cross section k_ν) and the second term represents the amount of radiation added to the beam (emission cross section j_ν). Defining the source function S_ν as the ratio of the emission cross section to the extinction cross section, we have

$$\frac{dI_\nu}{\rho \, k_\nu \, ds} = -I_\nu + S_\nu. \tag{2.9}$$

This is the *radiative transfer equation* and it governs the fundamental physics at work in the atmosphere. The simplistic form of the radiative transfer

equation hides its true complexity. The main problem lies in the nonlinearity of the equation. The solution of I_ν depends on j_ν, but if there is scattering in the atmosphere j_ν also depends on I_ν. A second problem lies in the definition of the source function $S_\nu = j_\nu/k_\nu$. The opacities that make up k_ν and j_ν can be composed of millions of lines for molecular species, and in the case of cloud opacities can involve a number of free parameters.

Finally, we can write Equation 2.9 in a more conventional form by making a few more definitions. If we consider a plane-parallel atmosphere, we are interested only in radiation flowing in the vertical direction z. We can define

$$\mu = \cos\theta, \tag{2.10}$$

where θ is again the angle measured from the vertical, or the zenith angle. The distance ds can be projected along the vertical axis, as in

$$ds = \cos\theta\, dz = \mu\, dz. \tag{2.11}$$

We can now define the *optical depth* τ as

$$\tau_\nu(z) = -\int_z k_\nu(z)\,\rho(z)\,dz. \tag{2.12}$$

The minus sign appears because the optical depth is by convention measured from the top of the atmosphere increasing downward. Using the definition of the optical depth, we can rewrite Equation 2.9 as

$$\mu\frac{dI_\nu}{d\tau} = I_\nu - S_\nu. \tag{2.13}$$

The detailed solution of this equation is beyond the scope of this work, and we refer the interested reader to more comprehensive works that describe the solution and application of the radiative transfer equation (e.g. Mihalas, 1970; Liou, 2002; Salby, 1996).

Fortunately, under specific assumptions, the solution to Equation 2.13 becomes simple. As discussed in Section 2.2, during transit the planet passes in front of the star, and some starlight passes through the annulus of the planetary atmosphere before reaching the observer. At visible wavelengths (where the thermal emission is negligible) the starlight is attenuated by the absorbing gases in the planet atmosphere. In this case, we take the emission, and thus the source function S_ν, to be zero, and Equation 2.13 reduces to

$$\mu\frac{dI_\nu}{d\tau} = I_\nu, \tag{2.14}$$

which can easily be integrated to obtain

$$I_\nu = I_\nu(0)\, e^{-\tau_\nu/\mu}. \tag{2.15}$$

This equation is known as Beer's Law or Lambert's Law (Liou, 2002). It describes the dissipation of radiation as it travels through a medium. Because atoms and molecules absorb at specific wavelengths, the amount of starlight that is trasmitted through the planetary atmosphere changes with wavelength.

Another physical situation with a simple solution to the radiative transfer equation is the case of thermal emission and no scattering. This situation would hold at infrared wavelengths if clouds (i.e. scattering particles) were not present. In this case of thermal emission, the source function is simply the blackbody function:

$$S_\nu = B_\nu \tag{2.16}$$

The radiative transfer equation (2.13) then reduces to a linear form:

$$\mu \frac{dI_\nu}{d\tau} = I_\nu - B_\nu. \tag{2.17}$$

The solution is

$$I_\nu(z) = \int_0^\pi \frac{1}{\mu} \int_0^\infty B_\nu(\tau) \exp^{-\tau_\nu(z)/\mu} d\tau d\mu. \tag{2.18}$$

With a given vertical temperature and pressure profile, the opacities and hence B_ν can be computed, and the right hand side of the above equation is straightforward to integrate.

2.6 Model Atmospheres

A full model atmosphere computation is needed to understand the details of the planetary spectrum. Usually the models assume that the planetary atmosphere is one-dimensional and plane-parallel (no curvature). The models produce the temperature and pressure as a function of altitude and the radiation field (that is, the emergent flux from the atmosphere) as a function of altitude and wavelength (see Seager *et al.* (2005) and references therein). To derive these three quantities, three equations are solved: the radiative transfer equation (Equation 2.13), the equation of hydrostatic equilibrium, and the radiative and convective equilibrium. The boundary conditions are the incident stellar radiation at the top of the atmosphere and the interior energy (assumed) at the bottom of the atmosphere. With this type of calculation, only the planetary surface gravity and the incident stellar radiation are known with certainty. Although the physics governing the model is relatively simple, a number of assumptions are necessary in order for the calculation to proceed, including (Seager *et al.*, 2005; Marley *et al.*, 2006):

- atmospheric chemistry (including elemental abundances, nonequilibrium chemistry, and photochemistry);
- cloud properties;
- atmospheric circulation;
- internal heat flow; and
- gaseous opacities.

Most published model results have typically used solar elemental abundances (i.e., having the same relative concentrations as the Sun.) Of course, this assumption is limited in that different stars will have relative abundances different from the Sun. Even the relative abundances of the elements in our Sun remain somewhat uncertain. More importantly, the solar system giant planets are enriched in carbon, and Jupiter and Saturn are also enriched in nitrogen relative to solar (see Marley *et al.* (2006) and references therein). With the assumed elemental abundances, chemical equilibrium calculations determine the abundances of the different atomic, molecular, and liquid or solid species as a function of temperature and pressure. For example, given the elemental abundances of carbon and oxygen relative to hydrogen, the relative concentrations of methane (CH_4) and carbon monoxide (CO) can be computed. CH_4 and CO are particularly interesting molecules for the hot Jupiters (Seager *et al.*, 2000) because it is unclear which one is the dominant form of carbon due to the uncertain temperatures and metallicities of the hot Jupiters. At higher temperatures and higher C to O ratios, we expect CO to be the dominant form of carbon, while at lower temperatures CH_4 is the dominant form of carbon.

With the computed abundances of chemical species, the opacities can be determined. The *opacity* represents the amount of radiation that a given species can absorb as a function of wavelength. The opacities of the expected chemical species in the model atmosphere play a pivotal role in determining the structure of the resulting spectrum. In particular, water, methane, ammonia (NH_3), sodium, and potassium all have significant spectral signatures for hot gas giant planets and are expected to be present in the atmospheres of these planets. Opacities are particularly sensitive to choices of metallicity, which species (atomic and molecular) are included, and whether equilibrium or non-equilibrium chemistry is considered. Absorption due to collisions between molecules (called Collision-Induced Absorption) also has a measurable effect, and modelers typically have to account for interactions between H_2–H_2 and H_2–He.

Cloud structure plays a critical role in controlling the resulting atmospheric spectra. Unfortunately, clouds are extremely difficult to model and

represent one of the greatest uncertainties in the atmospheric models. The structure, height, and composition of the clouds depends on the local conditions in the atmosphere as well as the transport (horizontal and vertical) of the condensates present in the atmosphere. In "ad hoc" cloud models, the type of condensates, the degree of condensation, and the particle size distribution are all free parameters in defining the cloud structure. One-dimensional cloud models use cloud microphysics to compute these parameters (Ackerman and Marley, 2001; Cooper *et al.*, 2003). All extrasolar planet atmosphere models currently in the literature further assume that the clouds are uniformly distributed over the entire planet.

Since the hot Jupiters are likely to be tidally locked (meaning the same hemisphere of the planet always faces the star), atmospheric circulation is key for redistributing absorbed stellar energy and determining the temperature gradients across the planet atmosphere. Atmospheric circulation models (e.g., Showman and Guillot, 2002; Cho *et al.*, 2003; Cooper and Showman, 2005) have not yet been coupled with radiative transfer models. In this absence, the atmospheric circulation has been parameterized by a parameter f: a value of $f = 1$ implies that the incident stellar radiation is emitted into 4π steradians (meaning the heat is evenly redistributed throughout the planet's atmosphere), while $f = 2$ implies that the incident stellar radiation is emitted into only 2π steradians (i.e., only the day side absorbs and emits the radiation, and there is no transport to the night side). This parameter is a way of quantifying the atmospheric dynamics, and it is used in the models to interpret the observed spectra (see Section 2.7). In model atmospheres this factor f is used in reducing the incident stellar radiation. It is also used in estimating the equilibrium temperature $T_{\rm eq}$, defined as

$$T_{\rm eq} = T_* \sqrt{\frac{R_*}{2a}} [f(1 - A_{\rm B})]^{1/4}, \tag{2.19}$$

where T_* is the stellar temperature, R_* is the stellar radius, a is the orbital semi-major axis, and $A_{\rm B}$ is the (unknown) Bond albedo, which is the fraction of incident stellar radiation scattered back into space in all directions by the planet. This relation was used to derived the values listed in Table 2.1, assuming $f = 1$ and $A_{\rm B} = 0.3$.

We now turn to a discussion of the specific spectroscopic and photometric observations of extrasolar planets that have been conducted.

2.7 Observations

In this section, we summarize the important spectroscopic and photometric observations of transiting planets that have been conducted, during both primary and secondary eclipse. Most of these observations have been performed on the planet HD 209458 b, since it was detected first. We conclude by describing how the model calculations have helped to interpret these results.

As discussed in Section 2.2, the planetary spectrum can be probed during transit using a method called transmission spectroscopy. Although the planetary spectrum is ~10,000 times fainter than that of the star, the differential nature of the measurement makes it possible to achieve this precision. Several detections and useful upper limits have been obtained on HD 209458 b:

- Sodium doublet detected (Charbonneau *et al.*, 2002);
- Hydrogen Lyman-α detected (Vidal-Madjar *et al.*, 2003);
- Carbon monoxide upper limit (Deming *et al.*, 2005a).

The sodium detected was approximately a factor of three smaller than expected from simple models of the atmosphere, suggesting the presence of a high cloud that masks the true sodium abundance. The detection of the transit in H Lyman-α was huge—a 15% drop in stellar flux during transit, 10 times greater than the transit depth at visible wavelengths. This implies an extended atmosphere of 3 or 4 Jupiter radii, and suggests that the planet is losing mass over its lifetime. The CO non-detection further reinforces the notion of a high cloud in the planet's atmosphere.

The complimentary technique during secondary eclipse is called *occultation spectroscopy*. Briefly, this involves taking spectra of the system when the planet is out of eclipse (when both the star and planet are visible) and comparing to spectra recorded when the planet is hidden during secondary eclipse. By carefully differencing these spectra, one can in principle derive the spectrum of the planet itself. Although this technique has not yet been successfully conducted on extrasolar planets, early attempts have yielded some useful information:

- Upper limit on emission near 2.2 μm (Richardson *et al.*, 2003b);
- Upper limit on methane abundance (Richardson *et al.*, 2003a).

Both of these limits were derived from ground-based observations, which are often limited by variations in the terrestrial atmosphere, making detection of spectral features difficult.

We now turn to photometric observations of the secondary eclipse that have occurred most recently. Although measurable, the effect due to the

secondary eclipse is small, e.g., ~0.3% for HD 209458 b at 20 μm (see Figure 2.2), and decreasing for smaller wavelengths. NASA's Spitzer Space Telescope† is responsible for the first detection of a secondary eclipse of a transiting planet. Spitzer, with an 85-cm aperture, has three instruments on board that together perform photometry and spectroscopy at infrared wavelengths. In March 2005, two independent research groups announced detections of the secondary eclipse of two different planets using two Spitzer instruments. Observations of HD 209458 b with the Multiband Imagaing Photometer for Spitzer (MIPS) detected the secondary eclipse at 24 μm (Deming *et al.*, 2005b), while TrES-1 was observed in two wavelengths (4.5 and 8 μm) with the Infrared Array Camera (IRAC) (Charbonneau *et al.*, 2005). These observations represent the first *direct* detection of an extrasolar planet. Most recently, the secondary eclipse of HD 189733 b was observed at 16 μm using the Infrared Spectrograph (IRS), although the observation was performed photometrically, not spectroscopically, using a detector that is normally used only to align the star on the slit (Deming *et al.*, 2006).

The secondary eclipse detections provide a measurement of the *brightness temperature* of the planets, at the respective wavelengths. The brightness temperature is the blackbody temperature of an object at a particular wavelength; given the irradiance, the blackbody function (see Equation 2.6) can be inverted to solve for temperature. For HD 209458 b the brightness temperature at 24 μm is 1130±150 K (Deming *et al.*, 2005b), and for TrES-1 it is 1010±60 K at 4.5 μm and 1230±110 K at 8 μm (Charbonneau *et al.*, 2005). HD 189733 b has a brightness temperature of 1117±42 K at 16 μm (Deming *et al.*, 2006). Although models have predicted the effective temperature of the atmospheres of extrasolar planets, these are the first observational measurements of the temperature of an extrasolar planetary atmosphere.

With the Spitzer photometry of several transiting planets, as well ground-based spectroscopic observations, we can now compare the observational results to theoretical calculations and begin to construct a comprehensive picture of the atmospheres of the transiting planets. In the wake of the three initial photometric detections of thermal emission from two extrasolar planets (Deming *et al.*, 2005b; Charbonneau *et al.*, 2005), *four* theory papers (Seager *et al.*, 2005; Barman *et al.*, 2005; Fortney *et al.*, 2005; Burrows *et al.*, 2005) appeared within a few months to explain the results! Some of these even have conflicting conclusions. One conclusion on which all of the explanations agree is that the planets are hot, as predicted. (We note that this was not a given; a planet with a high Bond albedo, for example, would

† `http://ssc.spitzer.caltech.edu/`

reflect much of the incident stellar irradiation and therefore could be much cooler, as seen in Equation 2.19.)

The second point on which all modelers agree is that the TrES-1 data points at 4.5 and 8.0 μm are not consistent with the assumption of solar abundances, because the 8.0 μm flux is too high. Beyond these two conclusions, the interpretations diverge.

Seager *et al.* (2005) conclude that a range of models remain consistent with the data. They include the 2.2 μm upper limit reported by Richardson *et al.* (2003b) (which has been largely ignored by modelers), as well as an upper limit on the albedo from the Canadian MOST satellite (Rowe *et al.*, 2005), and are able to eliminate the models for HD 209458 b that are on the hot and cold ends of the plausible temperature range for the planet. Their work suggests that an intermediate value for f (see Equation 2.19) is most likely, indicating that the atmospheric circulation is somewhere between the two extremes (efficient redistribution vs. none at all). The interpretation by (Seager *et al.*, 2005) and the observational results for HD 209458 b are shown in Figure 2.4.

Fortney *et al.* (2005) show that standard models using solar abundances are consistent with HD 209458 b but only marginally consistent (within 2σ at 8.0 μm) for TrES-1. For both planets, their best fit models assume that the incident stellar radiation is redistributed efficiently throughout the atmosphere (i.e., $f = 1$). On the other hand, Burrows *et al.* (2005) conclude that the $f = 2$ case is more likely, indicating that the day side is significantly brighter in the infrared than the night side. They also infer the presence of CO and possibly H_2O. The resolution of this discrepancy awaits further Spitzer observations.

Finally, with the recent Spitzer detection of HD 189733 b during secondary eclipse at 16 μm (Deming *et al.*, 2006) and detections by IRAC and MIPS under analysis (D. Charbonneau, private communication), we have more data available for comparison to theoretical spectra. In addition, observations are being analyzed or planned to detect a mid-infrared emission spectrum of HD 209485 b and HD 189733 b, respectively, both using Spitzer/IRS. These observations would be the first observed emission spectra of an extrasolar planet and will advance our understanding beyond the few photometric data points we have now.

2.8 Future Missions

The spectroscopic and photometric observations of hot Jupiters have provided a wealth of information on their physical characteristics and led to

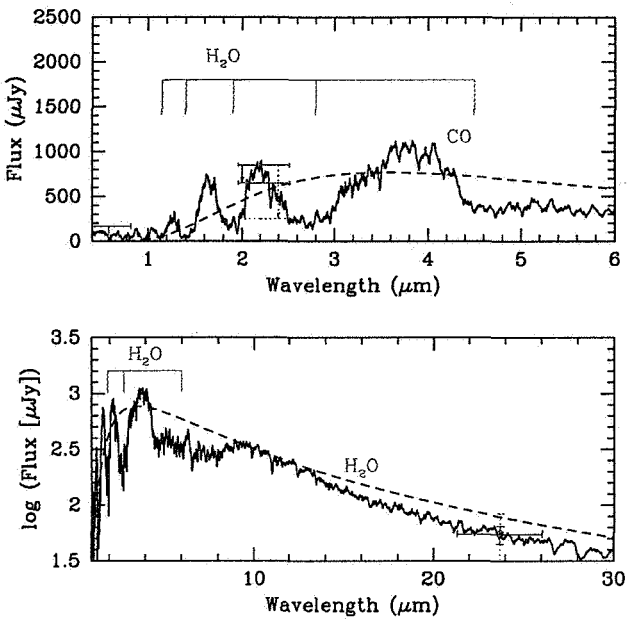

Fig. 2.4. Theoretical spectrum of HD 209458 b with data points and upper limits. The solid curve is a cloud-free model with solar abundances and $f = 2$, characterized by deep water vapor absorption features. From left to right the data points are: the MOST upper limit (Rowe *et al.*, 2005), a constraint on the H_2O band depth (Richardson *et al.*, 2003a; Seager *et al.*, 2005), and the Spitzer/MIPS thermal emission point at 24 μm (Deming *et al.*, 2005b). The solid lines show 1 σ error bars or upper limits and the dashed lines show 3 σ values. Note the linear flux scale on the upper panel and the log flux scale on the lower panel.

insights about their atmospheric structure. What about extrasolar planets similar to the Earth? Although detection of such rocky planets remains just beyond the limits of current detection techniques, a few short-period planets with masses only 5–15 times that of the Earth (sometimes called "hot super-massive Earths") have been discovered (Santos *et al.*, 2004; Beaulieu *et al.*, 2006), pushing the detection limit to ever-smaller planets. We close this chapter with a brief discussion of how we might search for Earth-like planets around other stars and what future missions are being planned to tackle this fundamental question.

The goal of directly imaging an Earth-like planet is to search for *biosignatures*, which are spectral features that can be used as diagnostics to search for the presence of life as we know it. The Earth has several such biosig-

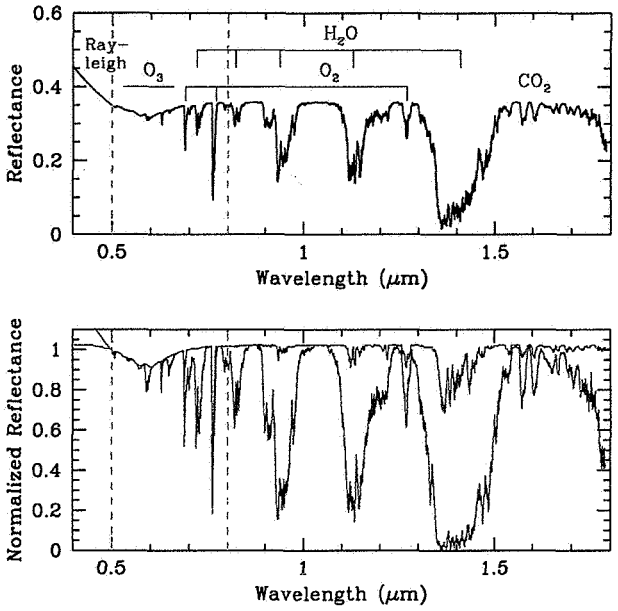

Fig. 2.5. Theoretical spectra of Earth. Upper panel: theoeretical model that matches the Woolf *et al.* (2002) Earthshine data. The dashed vertical lines show the nominal wavelength range of TPF-C. Lower panel: normalized models of Earth showing effects of clouds. The top curve is for uniform high cloud coverage showing weaker water vapor features. The bottom curve shows the case with no clouds, resulting in deep absorption features.

natures that are indicative of habitability or life. Figure 2.5 shows two of these species: O_2 and its photolytic product O_3, two of the most reliable biosignature gas indicators of life. O_2 is highly reactive and therefore will remain in significant quantities in the atmosphere only if it is continually produced. There are no abiotic continuous sources of large quantities of O_2 and only rare false positives that in most cases could likely be ruled out by other planetary characteristics. N_2O is a second gas produced by life—albeit in small quantities—during microbial oxidation-reduction reactions. N_2O has a very weak spectroscopic signature.

In addition to atmospheric biosignatures, the Earth has one very strong and very intriguing biosignature on its surface: vegetation. The reflection spectrum of photosynthetic vegetation has a dramatic sudden rise in albedo around 750 nm by almost an order of magnitude! (This effect is not included in the model plotted in Figure 2.5.) Vegetation has evolved this strong re-

flection feature, known as the 'red edge,' as a cooling mechanism to prevent overheating which would cause chlorophyll to degrade. On Earth, this feature is likely reduced by a few percent due to clouds. A surface biosignature might be distinguished from an atmospheric signature by observing time variations; that is, as the continents, for example, rotate in and out of view, the spectral signal will change correspondingly. Other spectral features, although not biosignatures because they do not reveal direct information about life or habitability, can nonetheless provide significant information about the planet. These include CO_2 (which is indicative of a terrestrial atmosphere and has a very strong mid-infrared spectral feature) and CH_4 (which has both biotic and abiotic origins). A range of spectral features is needed to characterize Earth-like planet atmospheres.

The James Webb Space Telescope (JWST) (e.g., Gardner *et al.*, 2006), tentatively scheduled for launch after 2013, will pick up where Spitzer leaves off, in terms of extrasolar planet characterization by primary and secondary eclipse studies. JWST is an infrared telescope with an aperture 6.5 m in diameter, representing a factor of $\sim$60 greater collecting area over Spitzer's 0.85 m diameter aperture. JWST will not only be able to detect thermal emission spectra from hot Jupiters, but also may be able to see emission from hot, super-massive Earths. It may also be possible to perform transmission spectroscopy on such planets with JWST.

NASA's Terrestrial Planet Finder (TPF) missions and ESA's Darwin mission seek to find and characterize Earth-like planets orbiting nearby stars. TPF is split into two separate missions, a visible coronograph (TPF-C) and an infrared nulling interferometer (TPF-I). Although scheduling and budgets for TPF are tentative, these missions would provide direct imaging of planets and thus low-resolution spectra of a wide variety of planet sizes and semi-major axes. One major goal of these missions would be to search the observed spectra for the biosignature features described above, in hopes of finding evidence for life on another world.

2.9 Summary

The transiting extrasolar planets have provided new opportunities to characterize the atmospheres and bulk compositions of worlds beyond our solar system. The geometry of these systems, in which the planet periodically crosses in front of its parent star (primary eclipse) and disappears behind the star (secondary eclipse), has allowed measurements of the true mass, radius, density, and (in a few cases) the brightness temperature of these planets for the first time. This chapter has also presented a brief overview

of spectroscopy, summarized how model atmospheres are computed, and described the notable observations of transiting planets. Finally, this chapter has addressed the detection and characterization of Earth-like planets around other stars and summarized a few missions being planned to accomplish this.

References

Ackerman, A. S., and Marley, M. S. (2001). Precipitating Condensation Clouds in Substellar Atmospheres. *Astrophys. J.*, **556**, 872-884.

Alonso, R., Brown, T. M., Torres, G. *et al.* (2004). TrES-1: The Transiting Planet of a Bright K0 V Star. *Astrophys. J. Lett.*, **613**, L153-L156.

Bakos, G. A., Pal, A., Latham, D. W., Noyes, R. W., and Stefanik, R. P. (2006). A stellar companion in the HD 189733 system with a known transiting extrasolar planet. *Arxiv astrophysics e-prints*, Feb.

Barman, T. S., Hauschildt, P. H., and Allard, F. (2005). Phase-Dependent Properties of Extrasolar Planet Atmospheres. *Astrophys. J.*, **632**, 1132-1139.

Beaulieu, J.-P., Bennett, D. P., Fouqué, P. *et al.* (2006). Discovery of a cool planet of 5.5 Earth masses through gravitational microlensing. *Nature*, **439**, 437-440.

Bouchy, F., Pont, F., Santos, N. C. *et al.* (2004). Two new "very hot Jupiters" among the OGLE transiting candidates. *Astron. Astrophys.*, **421**, L13-L16.

Bouchy, F., Udry, S., Mayor, M. *et al.* (2005). ELODIE metallicity-biased search for transiting Hot Jupiters. II. A very hot Jupiter transiting the bright K star HD 189733. *Astron. Astrophys.*, **444**, L15-L19.

Burrows, A., and Sharp, C. M. (1999). Chemical Equilibrium Abundances in Brown Dwarf and Extrasolar Giant Planet Atmospheres. *Astrophys. J.*, **512**, 843-863.

Burrows, A., Guillot, T., Hubbard, W. B. *et al.* (2000). On the Radii of Close-in Giant Planets. *Astrophys. J. Lett.*, **534**, L97-LL100.

Burrows, A., Sudarsky, D., and Hubbard, W. B. (2003). A Theory for the Radius of the Transiting Giant Planet HD 209458b. *Astrophys. J.*, **594**, 545-551.

Burrows, A., Hubeny, I., and Sudarsky, D. (2005). A Theoretical Interpretation of the Measurements of the Secondary Eclipses of TrES-1 and HD 209458b. *Astrophys. J. Lett.*, **625**, L135-L138.

Charbonneau, D. (2003). HD 209458 and the Power of the Dark Side. *Pages 449-456 of: Asp conf. ser. 294: Scientific frontiers in research on extrasolar planets.*

Charbonneau, D., Brown, T. M., Latham, D. W., and Mayor, M. (2000). Detection of Planetary Transits Across a Sun-like Star. *Astrophys. J. Lett.*, **529**, L45-L48.

Charbonneau, D., Brown, T. M., Noyes, R. W., and Gilliland, R. L. (2002). Detection of an Extrasolar Planet Atmosphere. *Astrophys. J.*, **568**, 377-384.

Charbonneau, D., Allen, L. E., Megeath, S. T. *et al.* (2005). Detection of Thermal Emission from an Extrasolar Planet. *Astrophys. J.*, **626**, 523-529.

Cho, J. Y.-K., Menou, K., Hansen, B. M. S., and Seager, S. (2003). The Changing

Face of the Extrasolar Giant Planet HD 209458b. *Astrophys. J. Lett.*, **587**, L117-L120.

Cooper, C. S., and Showman, A. P. (2005). Dynamic Meteorology at the Photosphere of HD 209458b. *Astrophys. J. Lett.*, **629**, L45-L48.

Cooper, C. S., Sudarsky, D., Milsom, J. A., Lunine, J. I., and Burrows, A. (2003). Modeling the Formation of Clouds in Brown Dwarf Atmospheres. *Astrophys. J.*, **586**, 1320-1337.

Deming, D., Brown, T. M., Charbonneau, D., Harrington, J., and Richardson, L. J. (2005). A New Search for Carbon Monoxide Absorption in the Transmission Spectrum of the Extrasolar Planet HD 209458b. *Astrophys. J.*, **622**, 1149-1159.

Deming, D., Seager, S., Richardson, L. J., and Harrington, J. (2005). Infrared radiation from an extrasolar planet. *Nature*, **434**, 740-743.

Deming, D., Harrington, J., Seager, S., and Richardson, L. J. (2006). Strong Infrared Emission from the Extrasolar Planet HD189733b. *Arxiv astrophysics e-prints*, Feb.

Fortney, J. J., Marley, M. S., Lodders, K., Saumon, D., and Freedman, R. (2005). Comparative Planetary Atmospheres: Models of TrES-1 and HD 209458b. *Astrophys. J. Lett.*, **627**, L69-L72.

Gardner, J. P., Mather, J. C., Clampin, M. *et al.* (2006). The James Webb Space Telescope. *Arxiv astrophysics e-prints*, June.

Gaudi, B. S., Seager, S., and Mallen-Ornelas, G. (2005). On the Period Distribution of Close-in Extrasolar Giant Planets. *Astrophys. J.*, **623**, 472-481.

Henry, G. W., Marcy, G. W., Butler, R. P., and Vogt, S. S. (2000). A Transiting "51 Peg-like" Planet. *Astrophys. J. Lett.*, **529**, L41-L44.

Holman, M. J., Winn, J. N., Stanek, K. Z. *et al.* (2005). High-precision Transit Photometry of OGLE-TR-10. *Arxiv astrophysics e-prints*, June.

Knutson, H., Charbonneau, D., Noyes, R. W., Brown, T. M., and Gilliland, R. L. (2006). Using Stellar Limb-Darkening to Refine the Properties of HD 209458b. *Arxiv astrophysics e-prints*, Mar.

Konacki, M., Torres, G., Sasselov, D. D. *et al.* (2004). The Transiting Extrasolar Giant Planet around the Star OGLE-TR-113. *Astrophys. J. Lett.*, **609**, L37-L40.

Konacki, M., Torres, G., Sasselov, D. D., and Jha, S. (2005). A Transiting Extrasolar Giant Planet around the Star OGLE-TR-10. *Astrophys. J.*, **624**, 372-377.

Laughlin, G., Wolf, A., Vanmunster, T. *et al.* (2005). A Comparison of Observationally Determined Radii with Theoretical Radius Predictions for Short-Period Transiting Extrasolar Planets. *Astrophys. J.*, **621**, 1072-1078.

Liou, K. N. (2002). *An Introduction to Atmospheric Radiation.* 2 edn. Academic Press.

Marley, M. S., Fortney, J., Seager, S., and Barman, T. (2006). Atmospheres of Extrasolar Giant Planets. *Arxiv astrophysics e-prints*, Feb.

Mazeh, T., Naef, D., Torres, G. *et al.* (2000). The Spectroscopic Orbit of the Planetary Companion Transiting HD 209458. *Astrophys. J. Lett.*, **532**, L55-L58.

McCullough, P. R., Stys, J. E., Valenti, J. A. *et al.* (2006). A Transiting Planet of a Sun-like Star. *Arxiv astrophysics e-prints*, May.

Mihalas, D. (1970). *Stellar Atmospheres.* W. H. Freeman and Company.

Moutou, C., Pont, F., Bouchy, F., and Mayor, M. (2004). Accurate radius and mass of the transiting exoplanet OGLE-TR-132b. *Astron. Astrophys.*, **424**, L31-L34.

Pont, F., Bouchy, F., Queloz, D. *et al.* (2004). The "missing link": A 4-day period transiting exoplanet around OGLE-TR-111. *Astron. Astrophys.*, **426**, L15-L18.

Richardson, L. J., Deming, D., Wiedemann, G. *et al.* (2003). Infrared Observations during the Secondary Eclipse of HD 209458b. I. 3.6 Micron Occultation Spectroscopy Using the Very Large Telescope. *Astrophys. J.*, **584**, 1053-1062.

Richardson, L. J., Deming, D., and Seager, S. (2003). Infrared Observations during the Secondary Eclipse of HD 209458b. II. Strong Limits on the Infrared Spectrum Near 2.2 Microns. *Astrophys. J.*, **597**, 581.

Rowe, J. F., Matthews, J. M., Seager, S. *et al.* (2005). MOST spacebased photometry of the transiting exoplanet system HD 209458: I. Albedo Measurements of an Extrasolar Planet. *American Astronomical Society meeting abstracts* **207**, -+.

Salby, M. L. (1996). *Fundamentals of Atmospheric Physics.* Academic Press.

Santos, N. C., Bouchy, F., Mayor, M. *et al.* (2004). The HARPS survey for southern extra-solar planets. II. A 14 Earth-masses exoplanet around μ Arae. *Astron. Astrophys.*, **426**, L19-L23.

Santos, N. C., Pont, F., Melo, C. *et al.* (2006). High resolution spectroscopy of stars with transiting planets. The cases of OGLE-TR-10, 56, 111, 113, and TrES-1. *Astron. Astrophys.*, **450**, 825-831.

Sato, B., Fischer, D. A., Henry, G. W. *et al.* (2005). The N2K Consortium. II. A Transiting Hot Saturn around HD 149026 with a Large Dense Core. *Astrophys. J.*, **633**, 465-473.

Seager, S., and Mallén-Ornelas, G. (2003). A Unique Solution of Planet and Star Parameters from an Extrasolar Planet Transit Light Curve. *Astrophys. J.*, **585**, 1038-1055.

Seager, S., Whitney, B. A., and Sasselov, D. D. (2000). Photometric Light Curves and Polarization of Close-in Extrasolar Giant Planets. *Astrophys. J.*, **540**, 504-520.

Seager, S., Richardson, L. J., Hansen, B. M. S. *et al.* (2005). On the Dayside Thermal Emission of Hot Jupiters. *Astrophys. J.*, **632**, 1122-1131.

Showman, A. P., and Guillot, T. (2002). Atmospheric circulation and tides of "51 Pegasus b-like" planets. *Astron. Astrophys.*, **385**, 166-180.

Torres, G., Konacki, M., Sasselov, D. D., and Jha, S. (2004). New Data and Improved Parameters for the Extrasolar Transiting Planet OGLE-TR-56b. *Astrophys. J.*, **609**, 1071-1075.

Vidal-Madjar, A., des Etangs, A. L., Désert, J.-M. *et al.* (2003). An extended upper atmosphere around the extrasolar planet HD209458b. *Nature*, **422**, 143-146.

Winn, J. N., and Holman, M. J. (2005). Obliquity Tides on Hot Jupiters. *Astrophys. J. Lett.*, **628**, L159-L162.

Winn, J. N., Noyes, R. W., Holman, M. J. *et al.* (2005). Measurement of Spin-Orbit Alignment in an Extrasolar Planetary System. *Astrophys. J.*, **631**, 1215-1226.

Woolf, N. J., Smith, P. S., Traub, W. A., and Jucks, K. W. (2002). The Spectrum of Earthshine: A Pale Blue Dot Observed from the Ground. *Astrophys. J.*, **574**, 430-433.